Article

A silicon-made microfluidic device for the fabrication of excipient-free pure drug nanoparticles

Roni Sverdlov Arzi [1], Asaf Kay [2], Yulia Raychman [1] and Alejandro Sosnik [1,*]

[1] Laboratory of Pharmaceutical Nanomaterials Science, Department of Materials Science and Engineering, Technion-Israel Institute of Technology, Haifa, Israel; ronisv@campus.technion.ac.il
[2] Laboratory of Electrochemical Materials and Devices, Department of Materials Science and Engineering, Technion-Israel Institute of Technology, Haifa, Israel; asaf.kay@gmail.com
* Author to whom correspondence should be addressed: sosnik@technion.ac.il, alesosnik@gmail.com; Tel.: +972-77-887-1971

Abstract: Nanoprecipitation by liquid anti-solvent precipitation is one of the most versatile methods to produce pure drug nanoparticles (PDNPs) owing to the ability to optimize the properties of the product. Nevertheless, nanoprecipitation shows broad particle size distribution and low physical stability, leading to high batch-to-batch variability and challenging the bench-to-bedside translation. Microfluidics has emerged as a powerful tool to produce PDNPs in a simple, reproducible, and cost-effective manner with excellent control over NP size. In this work, we designed and fabricated T- and Y-shaped Si-made microfluidics device and used it to produce pure NPs of three kinase inhibitors of different lipophilicity and water-solubility, namely imatinib, dasatinib and tofacitinib, without the use of colloidal stabilizers. PDNPs display sizes in the 90-350 nm range (dynamic light scattering) and a rounded shape (high-resolution scanning electron microscopy). Analysis by X-rays diffraction and differential scanning calorimetry confirmed that this method results in highly amorphous NPs. In addition, we show that the flow rate of solvent, the anti-solvent, and the channel geometry of the device play a key role in the size of the generated NPs.

Keywords: kinase inhibitors; pure drug nanoparticles; drug nanocrystals; bottom-up nanonization; nanoprecipitation; microfluidics; flow focusing technologies

1. Introduction

Nanotechnology has made a significant contribution to overcome (bio)pharmaceutical drawbacks of drugs such as poor aqueous solubility, low physicochemical stability in the biological milieu, short half-life and low bioavailability and efficacy [1–4]. For instance, >60% of the approved small-molecule drugs and ~90% of new drugs under development are classified as poorly water-soluble according to the Biopharmaceutics Classification System (BCS) [5–8]. These drawbacks lead to high drug attrition rates, making it difficult to translate drugs into new pharmaceutical products, and motivating the pharmaceutical industry to seek for non-traditional dosage forms and delivery routes [9–14].

Drug nanonization via top-down and bottom-up techniques has gained clinical impact [1,15–20] to increase the dissolution rate and saturation solubility due to reduction of the particle size and the associated increase of the specific surface area-to-volume ratio [15,21–23]. Top-down techniques involve the breakdown of large particles into smaller ones by mechanical forces (e.g., high pressure homogenization, wet ball milling) [19,20], whereas bottom-up techniques (e.g., nanoprecipitation, sono-crystallization, and drying technologies) produce the particles through precipitation from a solution at the nanometer scale. While the former are straightforward and reliable for industrial scale-up, the

latter offer great flexibility during the synthesis as well as improved control over the physicochemical characteristics of the product (e.g., particle size, morphology, amorphousness *versus* crystallinity) by adjusting the process conditions [10,24,25]. Additionally, bottom-up techniques enable the combination of more than one active pharmaceutical ingredient (API) in one single nanoparticle such in the case of drug-drug co-crystals [26,27].

Amid the nanotechnology-based products that have already been approved by US-Food and Drug Administration (FDA) for clinical use, pure drug nanoparticles (PDNPs) within a size range from a few nanometers up to 1 μm are the simplest and most patented technology to increase the water dissolution rate of hydrophobic drugs and increase their oral bioavailability [28–32]. PDNPs have been also used in the development of long-acting injectable formulations [33] and their ability to increase the adhesion to the intestinal mucosa and prolong the residence time in the gut with respect to microparticles has been reported [16,29]. PDNPs have been also intended for targeted drug delivery by the intravenous route [34].

One of the most straightforward bottom-up techniques to produce these particles is by liquid anti-solvent precipitation that enables the fast, simple and energy-efficient formation of a wide range of nanomaterials [1,30,35–38]. However, the successful translation of nanoparticle formulations using conventional nanoprecipitation techniques still faces challenges, including the difficulty to control the size and the size distribution of the particles, their physicochemical instability in suspension (tendency to agglomerate), and the batch-to-batch variability due to the lack of control over the mixing process in the solution bulk [37,39,40]. The incorporation of colloidal stabilizers (e.g., surfactants) is often required to control the drug particle growth and prevent particle agglomeration and thus, increase the physical stability of the nanosuspensions [41–44]. The incorporation of surfactants in the production process results in a smaller amount of API in the final product [34] and, in some cases, they have been associated with toxicity and side-effects [4,27].

Microfluidics emerged as a powerful tool in biology and nanomedicine in general [45–48] and pharmaceutical sciences in particular to synthesize surfactant-free PDNPs with controlled size and improved physical stability by the manipulation of fluids in micrometric channels/capillaries networks [39,40,49–53]. The precipitation process takes place inside the channels where the solvent (S) and anti-solvent (AS) are rapidly mixed, allowing precise liquid handling and uniform mass transfer, which in turn enables superior control over the features of the produced particles [22,54–56]. The mixing rate inside the channels is determined by the diffusion rate of the molecules across the interface and between the two fluids subjected to a continuous flow [51,57]. Another advantage of microfluidics is that the amount of reagents used for synthesis is very small, making this platform extremely cost-effective, especially in early pharmaceutical research and development (R&D) stages [40,58]. Owing to the controlled nature of this technique, particle size can be optimized by changing the conditions of the precipitation process (e.g., channel geometry, precursor composition, flow rate) [27,59].

Protein phosphorylation is the most common form of reversible post-translational modification and it is controlled by kinases [60] and kinase signaling pathways have been shown to drive many of the hallmark phenotypes of tumor biology, including proliferation, survival, motility, metabolism, angiogenesis, and evasion of antitumor immune responses. Kinase inhibitors belong to the so-called molecularly-targeted anticancer therapies and they emerged as one of the most intensively pursued targets [61,62]. To date, >40 small-molecule kinase inhibitors have been approved by the FDA for the therapy of cancer and, more recently, of autoimmune diseases such as rheumatoid arthritis and inflammatory bowel diseases [63]. In addition, >100 compounds are under clinical trials [61]. Many kinase inhibitors display poor aqueous solubility and moderate to low oral bioavailability

which jeopardizes their pharmacokinetics [64]. Others display a pH-dependent dissolution profile that results in differential precipitation along the gastrointestinal tract. Kinase inhibitors are administered by the oral route though a few studies proposed their use also by injection [65,66] for local therapy. Nanonization of pure kinase inhibitor nanoparticles emerges as a clinically relevant technological strategy not only to improve their oral bioavailability but to also take advantage of alternative administration routes (e.g., intranasal) to target brain tumors [67,68].

In this study, we report on the design and fabrication of simple Y- and T-shaped Si-made microfluidic devices by using photolithography and demonstrate its use to produce surfactant-free physically stable pure amorphous nanoparticles of three kinase inhibitors, namely imatinib (IMA), dasatinib (DAS) and tofacitinib (TOF) via a controlled nanoprecipitation process.

2. Materials and Methods

2.1. Materials

IMA free base and DAS free base monohydrate were supplied by Carbosynth Ltd. (Compton, UK) and TOF free base by LC Laboratories (Woburn, MA, USA). Ethanol, isopropanol, and acetone were purchased from Bio-Lab Ltd. (Jerusalem, Israel). Milli-Q water was obtained from a Barnstead Smart2Pure 12L UV/UF water purification system (Thermo Electron LED GmbH, Niederelbert, Germany). All the solvents were of analytical and spectroscopic grade and used as received.

2.2. Components of the microfluidic system

Silicon wafer was purchased from UniversityWafer, Inc. (Boston, MA, USA), polytetrafluoroethylene tubing from Wirtham Marketing & Suppliers (Haifa, Israel), and AZ 4533® and AZ 4562® photoresists from MicroChemicals GmbH (Ulm, Germany). The mask made of quartz coated with a thin layer of chromium was designed using AutoCAD® 22.0 software (Autodesk, Inc., San Rafael, CA, USA).

2.3. Methods

2.3.1. Design and assembly of the microfluidic device

The mask for the microfluidic channels was assembled using a computer-aided design and drafting software AutoCAD®. The width and depth of the channels were 500μm, with two different channel configurations, T- and Y-shaped. The length of the inlet and outlet channels in the T-shaped device were 15 and 8 mm, respectively, while in the Y-shaped one, they were 10 and 8 mm (Figure 1a).

For the lithographic process, a piece of p-type Si wafer <100> was sliced, cleaned in acetone, isopropanol, and water, and dried in dry air. Before dicing the wafer to its final dimensions (9.5 x 9.5 cm), the substrate was coated with AZ 4533® photoresist to protect the mask. Then, the substrate was cleaned and spin-coated to apply a thin layer of AZ 4562® photoresist by centrifugal force. After evaporation of the solvents in the photoresist via soft baking, the substrate was exposed to UV light through the mask with the microfluidic pattern. After baking, the exposed layer of the photoresist was removed using chemical bath development. Finally, dry reactive ion etching was performed to generate the channels and the Si piece was diced into rectangles and further cleaned. The system was assembled into three layers: the upper and lower layers were made of glass for mechanical strength and transparency and the middle layer was made of a Si wafer with the embedded T- and Y-shaped channels. Si was chosen owing to its good chemical compatibility and excellent thermal and mechanical stability under flow and pressure. The top layer was glued using Epo-Tek® 301 (Epoxy Technology Inc., MA, US) and the bottom and middle layers were glued together using Araldite® (Basel, Switzerland).

2.3.2. Production of pure additive-free kinase inhibitor nanoparticles

The overall experimental device consisted of a Si chip, two continuous infusion pumps (SYP-01, MRC Ltd., Holon, Israel) for supplying the drug solution in ethanol and water (used as AS), and a unit for the collection of the PDNPs in suspension. The setup is schematically illustrated in Figure 1b. To produce the PDNPs, each pristine drug was dissolved in ethanol (1 mL, final drug concentration was 0.1% w/v). Ethanol was chosen as the solvent (S) because it dissolves well all three drug candidates, it is miscible with the AS and it can be eliminated by evaporation at room temperature (RT) and atmospheric pressure. Moreover, ethanol is classified as Class III (solvents with low toxic potential) and is regarded as safe in relatively high amounts (daily exposure of up to~50 mg/day) by the International Conference on Harmonization [69]. Next, the drug solution (organic phase) and water (aqueous phase) were injected by two syringe infusion pumps into the channels of a T- or Y-shaped microfluidic device and mixed rapidly in the intersection point at RT to produce the nanoparticles. The size of the particles was controlled by varying the following process conditions: channel geometry, the overall flow rate of each phase and the S/AS volume ratio. Once the precipitation process was completed, the nanosuspension was immediately frozen at -80 °C and freeze-dried (Labconco Free Zone 4.5 plus L Benchtop Freeze Dry System, Labconco, Kansas City, MO, USA) for further characterization.

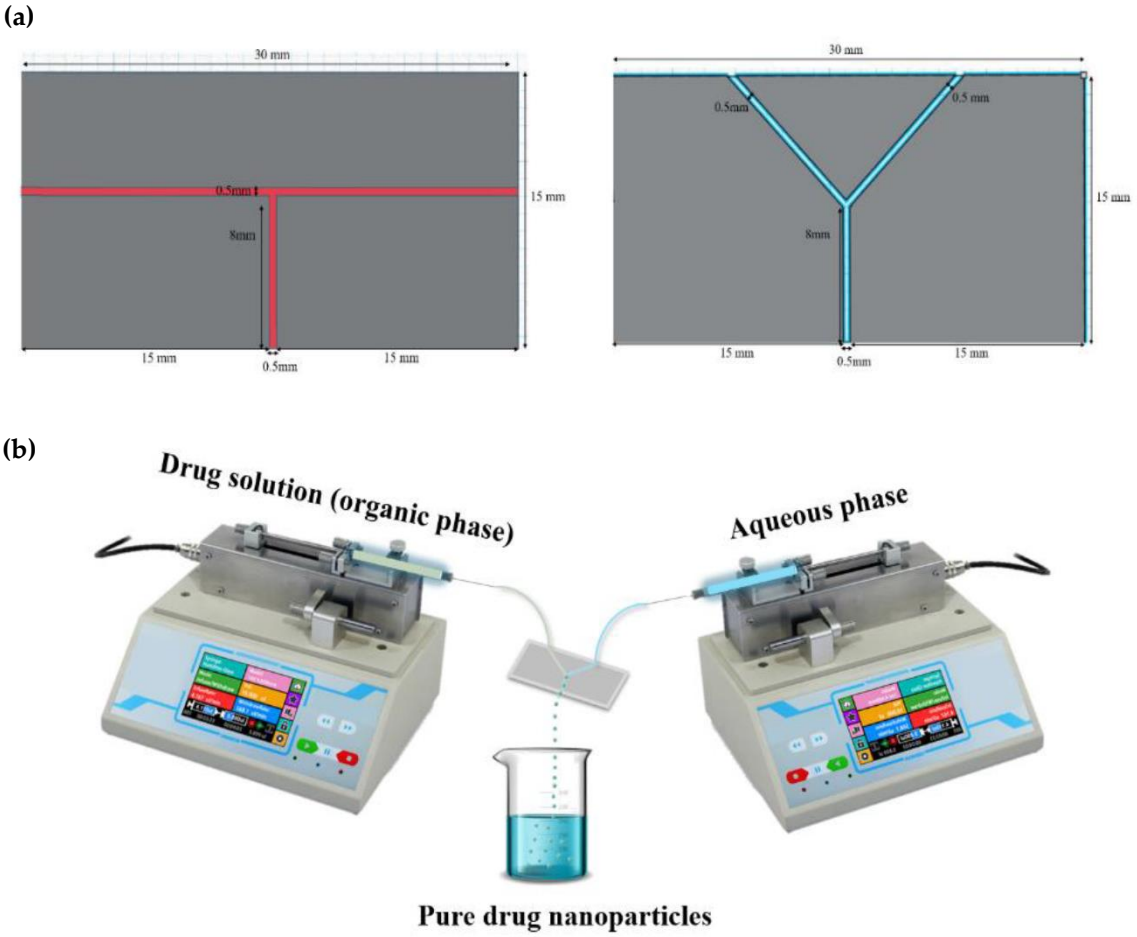

Figure 1. Scheme of (a) the T- and Y-shaped Si-made microfluidic devices and their dimensions and (b) the drug nanoprecipitation method using a Si-made Y-shaped microfluidic device. A similar process is conducted with a T-shaped chip.

2.3.3. Characterization of pristine drugs and pure drug nanoparticles

The hydrodynamic diameter (D_h), the polydispersity index (PDI, an estimation of the particle size distribution) and the zeta-potential (Z-potential) were determined in a Zetasizer Nano-ZS (Malvern Instruments, Malvern, UK) at 25 °C with a 4 mW He–Ne laser (λ = 633 nm), a digital correlator ZEN3600 and Non-Invasive Back Scatter (NIBS®) technology at a scattering angle of 173° to the incident beam. D_h and PDI were measured using the dynamic light scattering (DLS) technique. DLS data was analyzed using CONTIN algorithms (Malvern Instruments). Z-potential analysis used of laser Doppler microelectrophoresis in the same instrument. Values are expressed as mean ± standard deviation (S.D.) and each measurement were a result of at least five runs. The S.D. of each size population, which is an expression of the peak width, was also determined. Differences among particle sizes were analyzed using one-way analysis of variance (ANOVA, significance level of 1%) with Bonferroni test ($P < 0.01$).

The morphology of the different PDNPs was visualized by high resolution-scanning electron microscopy (HR-SEM, carbon coating, acceleration voltage of 1-4 kV, Ultraplus, Zeiss, Oberkochen, Germany). For HR-SEM, the pristine drugs and PDNP suspensions were dispersed in water and sprayed on top of a p-doped Si wafer <100> by introducing high pressure N_2, allowing the individual particles to be spread evenly on the wafer. Then, the wafer was attached to the grid using carbon-tape and additional tape was placed on its frame. Silver paint (Structure Probe, Inc., West Chester, PA, USA) was applied to the corners of the frame prior to carbon coating.

The structure (crystalline *versus* amorphous) of the PDNPs was analyzed by powder X-ray diffraction (PXRD) in an XRD diffractometer MiniFlex (Rigaku, Tokyo, Japan) under parallel-beam geometry at a speed rate of 6, θ-2θ range of 5-50° (with intervals of 0.01°) on a poly(methyl methacrylate) slide and RT. Diffractograms of the PDNPs were compared to those of the pristine drugs

Thermal characterizations were performed by differential scanning calorimetry (DSC, 2 STARe system equipped with a simultaneous thermal analyzer, STARe Software V13 and intra-cooler Huber TC100, Metter Toledo, Schwerzenbach, Switzerland). For this, samples (5-10 mg) sealed in 40 µL-Al crucible pans (Mettler Toledo) were heated from 25 to 325 °C at a heating rate of 10 °C/min under N_2 gas flow (20 mL/min) and In was used as a standard.

3. Results and Discussion

3.1. Rationale

To investigate the robustness of our microfluidic device to synthesize surfactant-free pure kinase inhibitor NPs, we selected three compounds (in free base form) with a broad range of octanol–water partition coefficient (logP) values and intermediate to low intrinsic water solubility (S_0) at neutral pH and 25°C. IMA (S_0 = 2 µg/mL, calculated logP = 4.53, Figure 2a) [70,71] was the first FDA-approved kinase inhibitor that targets the Bcr-Abl tyrosine kinase and the phosphorylation of the platelet derived growth factor receptor and it is used for the treatment of chronic myeloid leukemia. Its oral bioavailability is 98% [62]. DAS (S_0 = <1 µg/mL, logP = 3.83, Figure 2b) [70,72] is a dual Bcr-Abl and Src tyrosine kinase inhibitor used in chronic myelogenous leukemia and acute lymphoblastic leukemia with an oral bioavailability of 14% and 34% in mouse and dog, respectively [73]. Intravitreal DAS injection has been proposed in the treatment of ocular diseases [65,74]. TOF (S_0 = <300 µg/mL, calculated logP = 1.19, Figure 2c) [70,72,75] is a Janus kinase inhibitor approved for the treatment of rheumatoid and psoriatic arthritis and ulcerative colitis and displays an oral bioavailability of 74% [76,77].

Pure kinase inhibitor NPs were produced, and the effect of the physicochemical properties and the process conditions comparatively characterized. Initially, each pristine drug was

dissolved in ethanol (solvent, S) and the drug solution and water (anti-solvent, AS) were pumped via two infusion pumps into the two inlets of the microfluidic device and rapidly mixed inside the intersection point to ensure the controlled formation of the nanoparticles. To reach a yield of ~100%, we did not perform a filtration step after the nanoprecipitation. Moreover, to maximize the drug content in the final product, we produced the nanoparticles without a colloidal stabilizer to minimize the surface area and the free energy of the colloidal system, which was challenging because PDNPs tend to aggregate in suspension and grow over time [9]. After the nanoprecipitation, samples were frozen at -80 °C and freeze-dried for characterization.

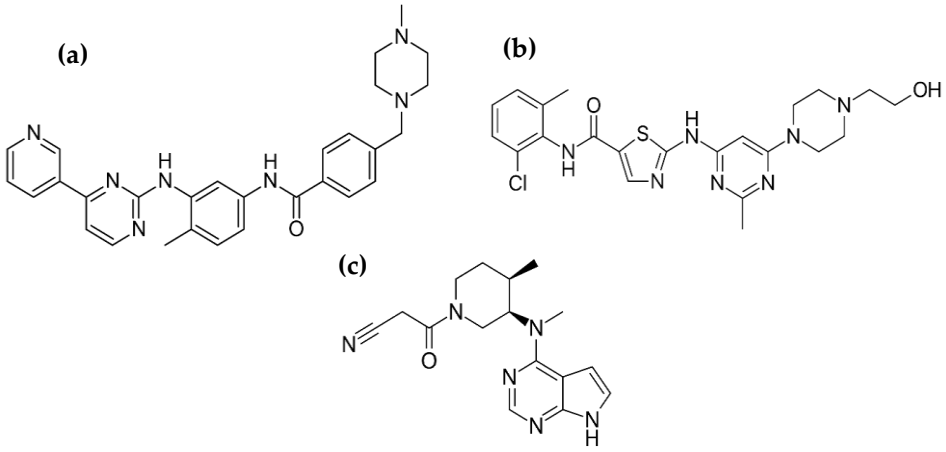

Figure 2. Chemical structure of (a) imatinib, (b) dasatinib and (c) tofacitinib (as free base).

3.2. Production and characterization of additive-free pure kinase inhibitor nanoparticles

Initial studies focused on the effect of different system parameters on particle size and size distribution using the Y- and T-shaped microfluidic devices to optimize the size of the synthesized nanoparticles. In this framework, the effect of the S and AS flow rates and the variation in the AS flow rate at constant S flow rate on the particle size were assessed. Results are summarized in Table 1 and Figure 3. The drug concentration of all drugs in ethanol was 0.1% w/v and we kept constant the S/AS volume ratio (1/10). All the experiments were conducted at 25 °C.

Table 1. Effect of the flow rate on the pure drug nanoparticle size using T- and Y-shaped devices and a fixed drug solution concentration of 0.1% w/v, as measured by DLS.

Drug	S/AS Flow Rate, (mL min^{-1}/mL min^{-1})	S/AS Volume Ratio	T-Shaped			Y-Shaped		
			D_h (nm) [1] (± S.D.)	S.D. (nm) [2]	PDI (nm) (± S.D.)	D_h (nm) [1] (± S.D.)	S.D. (nm) [2]	PDI (nm) (± S.D.)
IMA	0.05/0.5	1/10	196 (6)	75	0.13 (0.02)	143 (4)	53	0.18 (0.03)
	0.1/1.0		174 (9)	71	0.16 (0.01)	120 (12)	67	0.31 (0.01)
	0.2/2.0		133 (5)	60	0.30 (0.03)	146 (16)	50	0.24 (0.04)
	0.3/3.0		129 (5)	64	0.32 (0.02)	118 (7)	59	0.33 (0.05)
	0.4/4.0		91 (6)	37	0.30 (0.03)	107 (16)	60	0.30 (0.08)
	0.5/5.0		125 (4)	30	0.30 (0.03)	120 (3)	40	0.09 (0.02)
	0.6/6.0		160 (7)	66	0.20 (0.04)	90 (6)	38	0.30 (0.03)
	0.8/8.0		159 (12)	79	0.24 (0.02)	181 (7)	102	0.21 (0.00)
DAS	0.05/0.5		221 (10)	7	0.11 (0.01)	249 (14)	64	0.04 (0.01)
	0.1/1.0		223 (15)	49	0.20 (0.03)	162 (10)	60	0.15 (0.03)
	0.2/2.0		203 (6)	64	0.10 (0.00)	199 (6)	63	0.09 (0.02)
	0.3/3.0		184 (13)	44	0.02 (0.00)	181 (4)	52	0.07 (0.03)
	0.4/4.0		202 (39)	17	0.10 (0.05)	226 (26)	4	0.07 (0.02)
	0.5/5.0		213 (16)	5	0.05 (0.04)	210 (33)	9	0.04 (0.03)
	0.6/6.0		271 (21)	93	0.13 (0.00)	310 (10)	97	0.15 (0.07)
	0.8/8.0		243 (6)	72	0.12 (0.04)	316 (36)	82	0.05 (0.01)
TOF	0.05/0.5		188 (8)	54	0.31 (0.06)	174 (4)	78	0.20 (0.02)
	0.1/1.0		144 (10)	66	0.23 (0.05)	153 (6)	40	0.20 (0.02)
	0.2/2.0		99 (9)	22	0.43 (0.14)	108 (16)	26	0.34 (0.09)
	0.3/3.0		146 (15)	24	0.32 (0.07)	117 (16)	39	0.24 (0.07)
	0.4/4.0		130 (7)	52	0.32 (0.07)	114 (8)	65	0.30 (0.03)
	0.5/5.0		172 (17)	54	0.32 (0.00)	121 (10)	50	0.40 (0.08)
	0.6/6.0		148 (34)	28	0.50 (0.10)	143 (12)	70	0.32 (0.10)
	0.8/8.0		148 (20)	29	0.60 (0.20)	165 (17)	79	0.30 (0.06)

[1] D_h are the intensity distribution values expressed as the average of 5 runs (n = 5) ± S.D, as determined by DLS.

[2] Standard deviation (S.D.) of each size population that is an expression of the peak width, as determined by DLS.

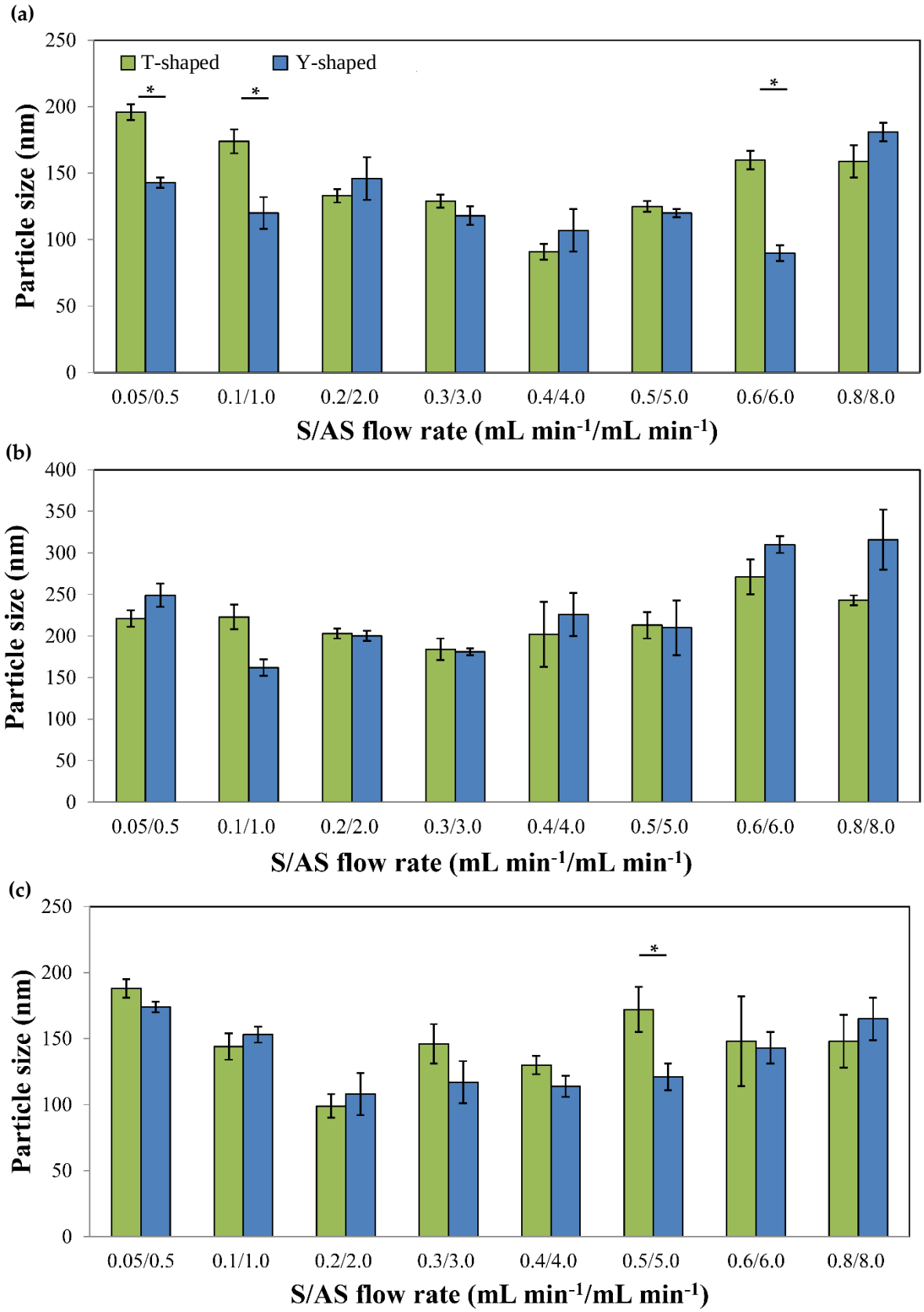

Figure 3. Effect of S/AS flow rate changes on the size of pure (a) imatinib (IMA), (b) dasatinib (DAS) and (c) tofacitinib (TOF) nanoparticles produced by using T- and Y-shaped devices, as measured by DLS at 25°C. A constant S/AS volume ratio of 1/10 was used. * Denotes statistically significant difference in the nanoparticle size between the two channel geometries ($P < 0.01$).

Following the change in the overall flow rate of the S and AS, the size of the PDNPs ranged from 80-200 nm, 170-350 nm and 90-190 nm for IMA, DAS and TOF, respectively (Table 1). DLS results showed that at the limits of low and high S/AS flow rates, the size of the particles was larger than the sizes obtained at intermediate flow rates. For example, the size of pure IMA NPs produced in the T- and Y-shaped devices decreased from 196 ± 6 and 143 ± 4 nm to 91 ± 6 and 107 ± 16 nm at flow rates of 0.05/0.5 and 0.4/4.0 mL min^{-1}/mL min^{-1}, respectively (Figure 3). A similar trend was observed for DAS and TOF NPs. This trend could be explained by the delicate interplay between efficient versus incomplete mixing of the S and the AS during the precipitation process. Micro-mixing (i.e., mixing at the molecular scale) is a key factor in determining the degree of the supersaturation of the drug and its local spatial distribution [57]. Subsequently, when the overall flow rate is increased the mass-transfer inside the channels is accelerated, generating a uniform spatial concentration distribution and localized supersaturated zones, that lead to the formation of smaller particles with narrower particle size distributions [52,78,79]. However, when the flow rate exceeded a certain limit, which can slightly differ from drug to drug based on its physicochemical properties and lipophilicity, micro-mixing becomes less homogeneous, accelerating the formation of larger particles characterized by broader size distributions [37,80,81]. It is clear from the results that the mixing stage is crucial in the determination of the final size of the particles, and that increasing the overall flow rate is beneficial only when complete mixing of the fluids is achieved.

Regarding the geometry of the channels (T- and Y-shaped), we anticipated differences in the flow pattern between the two shapes due to the difference in the inlet angle. In the T-shaped system, the inlet angle is larger (90°) and the two fluids that meet in the junction are more likely to disrupt each other as they flow by creating stagnant zones. Contrarily, in the Y-shaped system, the inlet angle is smaller (67.5°) and hence at lower flow rates the laminar flow of the S and AS is less disrupted [54]. Significant differences in particle size were observed between the two device geometries for IMA at the limits of low and high S/AS flow rate (0.05/0.5, 0.1/1.0 and 0.6/6.0 mL min^{-1}/mL min^{-1}) and for TOF at a flow rate of 0.5/5.0 mL min^{-1}/mL min^{-1} (Figure 3a and Figure 3c). In both cases smaller particles were produced by the Y-shaped system. Furthermore, at a higher flow rate of 0.8/8.0 mL min^{-1}/mL min^{-1}, the particle size difference between the two geometries was not observed for neither IMA nor TOF, probably due to the enhanced mixing at a higher flow rate (higher Reynolds number), reducing the effect of flow disturbance in the T-shaped device. In the case of pure DAS NPs, the particle size was not influenced significantly by the difference in the geometry of the devices under the same precipitation conditions (Figure 3b). Next, we kept the S flow rate constant at 0.5 mL min^{-1}, varied the AS flow rate from 3.5 to 6 mL min^{-1} and studied the effect of the variation of the AS flow rate with respect to the S flow rate on the size of the PDNPs by using the Y-shaped device. The results are summarized in Table 2 and Figure 4.

Table 2. Effect of anti-solvent injection rate on the size of the pure drug nanoparticles produced with a 0.1% w/v drug solution in ethanol by using a Y-shaped device, as measured by DLS at 25°C.

Drug	S/AS Volume Ratio	S/AS Flow Rate (mL min^{-1}/mL min^{-1})	D_h (nm) [1] (± S.D.)	S.D. (nm) [2]	PDI (nm) (± S.D.)
IMA	1/7	0.5/3.5	121 (13)	48	0.21 (0.08)
	1/8	0.5/4.0	91 (9)	26	0.20 (0.06)
	1/9	0.5/4.5	95 (9)	31	0.20 (0.05)
	1/10	0.5/5.0	121 (2)	40	0.10 (0.02)
	1/11	0.5/5.5	115 (4)	40	0.30 (0.02)
	1/12	0.5/6.0	124 (23)	32	0.20 (0.06)
DAS	1/7	0.5/3.5	210 (50)	22	0.06 (0.04)
	1/8	0.5/4.0	215 (29)	7	0.04 (0.02)
	1/9	0.5/4.5	215 (30)	17	0.05 (0.01)
	1/10	0.5/5.0	210 (19)	33	0.09 (0.06)
	1/11	0.5/5.5	255 (34)	17	0.05 (0.03)
	1/12	0.5/6.0	201 (18)	7	0.04 (0.03)
TOF	1/7	0.5/3.5	114 (6)	52	0.40 (0.15)
	1/8	0.5/4.0	96 (6)	49	0.30 (0.06)
	1/9	0.5/4.5	113 (12)	65	0.40 (0.04)
	1/10	0.5/5.0	107 (26)	61	0.30 (0.03)
	1/11	0.5/5.5	209 (29)	105	0.40 (0.15)
	1/12	0.5/6.0	180 (47)	56	0.45 (0.10)

[1] D_h are the intensity distribution values expressed as the average of 5 runs (n = 5) ± S.D, as determined by DLS.
[2] Standard deviation (S.D.) of each size population that is an expression of the peak width, as determined by DLS.

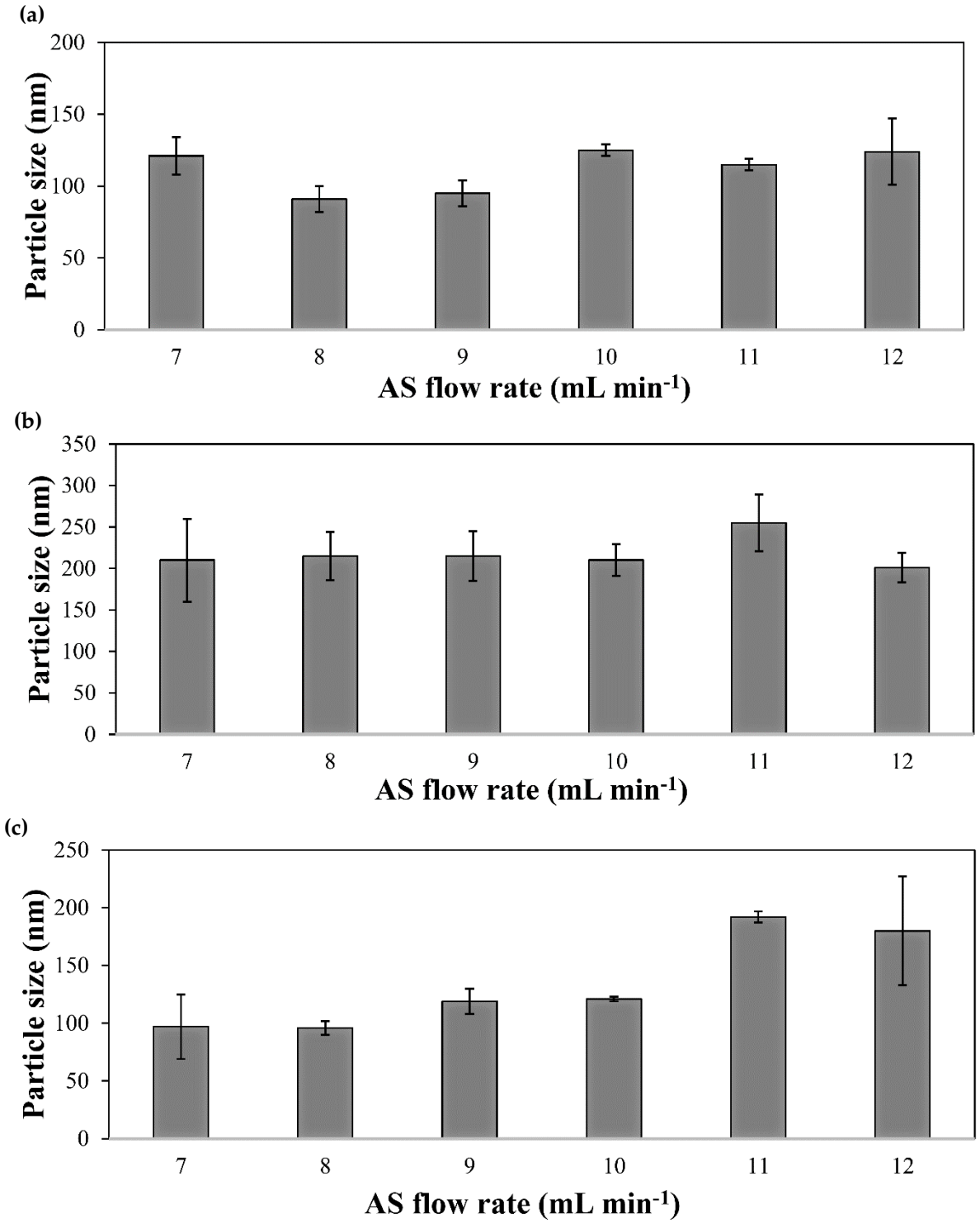

Figure 4. Effect of variation of AS flow rate on the size of pure drug nanoparticles produced by using a Y-shaped device, as measured by DLS at 25°C.

Since the driving force behind the initiation of the precipitation process is the supersaturation of the S induced by the rapid mixing with the AS, we expected that higher AS flow rates will generate a homogenous nucleation that would lead to the formation of smaller particles [9,57]. However, this was not the case. Pure DAS and IMA NPs did not show an apparent change in particle size with increasing AS flow rate. Pure TOF NPs showed the opposite trend where faster AS flow rate resulted in a significant increase of the particle size that could be attributed to incomplete mixing of the fluids with increasing water flow, resulting in to the formation of larger particles with broader particle size distributions [82,83]. The latter PDNPs also showed larger PDI

values compared to the IMA and DAS counterparts, possibly due to the more metastable nature of the nanonized TOF form which could be attributed to its lower lipophilicity [84].

Upon optimization of the process conditions, pure kinase inhibitor NPs were produced and thoroughly characterized them. For this, additive-free PDNPs were synthesized using the T-shaped device by setting flow rates of 0.2 and 2.0 mL min^{-1} for the S and AS, respectively.
Z-potential estimates the particle surface charge density, and it depends on the size of the particle and the concentration of charged moieties on the particle surface, which is directly related to the pH of the medium. The absolute Z-potential value could be associated to the physical stability of the colloidal system [85]. In this work, nanosuspensions were prepared in water with a pH value of ~5. Pure IMA, DAS and TOF showed moderately negative Z-potential values of -18 ± 2, -18 ± 3 and -31 ± 3 mV, respectively. The negative Z-potential of all the PDNPs was probably associated with the exposure of electronegative moieties (e.g., carbonyl) at the nanoparticle surface. In addition, the more negative value shown by TOF with respect to IMA and DAS would stems from the electronegativity of the nitrile functional group.

The dissolution rate of PDNPs is not only governed by the size of the particle but also by the crystalline/amorphous state of the drug. Usually, the dissolution rate of amorphous drugs is faster than that of the crystalline counterpart [86]. In addition, drug amorphization can also result in greater saturation solubility. To assess the state of the three drugs upon nanonization, we analyzed their diffraction pattern by PXRD and compared it to the unprocessed counterparts. In general, the pristine drugs showed crystalline or semi-crystalline structure, and they underwent substantial amorphization upon nanonization, as clear from the broadening and, in some cases the disappearance, of the diffraction peaks that are characteristic of the crystalline drug (Figure 5). For example, in the diffractogram of TOF, the raw drug showed a considerably high crystallinity as demonstrated by a series of sharp and intense diffraction peaks in accordance with literature [87]. Conversely, nanonized TOF formed a halo pattern typical of a substantially amorphous material, with the exception of two peaks at $2\theta = 31.7$ and $2\theta = 45.5$ that were not observed in the XRD pattern of raw TOF (Figure 5c). The appearance of the new peaks suggests that the drug underwent changes during nanonization which may have led to the formation of a different drug polymorph (Figure 5c) [88].
It should be noted that in our work PDNPs are frozen and freeze-dried immediately after synthesis, and both quenching and drying could explain the amorphous nature of the NPs. Amorphous PDNPs could be preferred over crystalline ones to achieve faster dissolution rate of poorly water-soluble compounds under physiological conditions. On the other hand, amorphous drugs are usually less chemically stable [89,90].

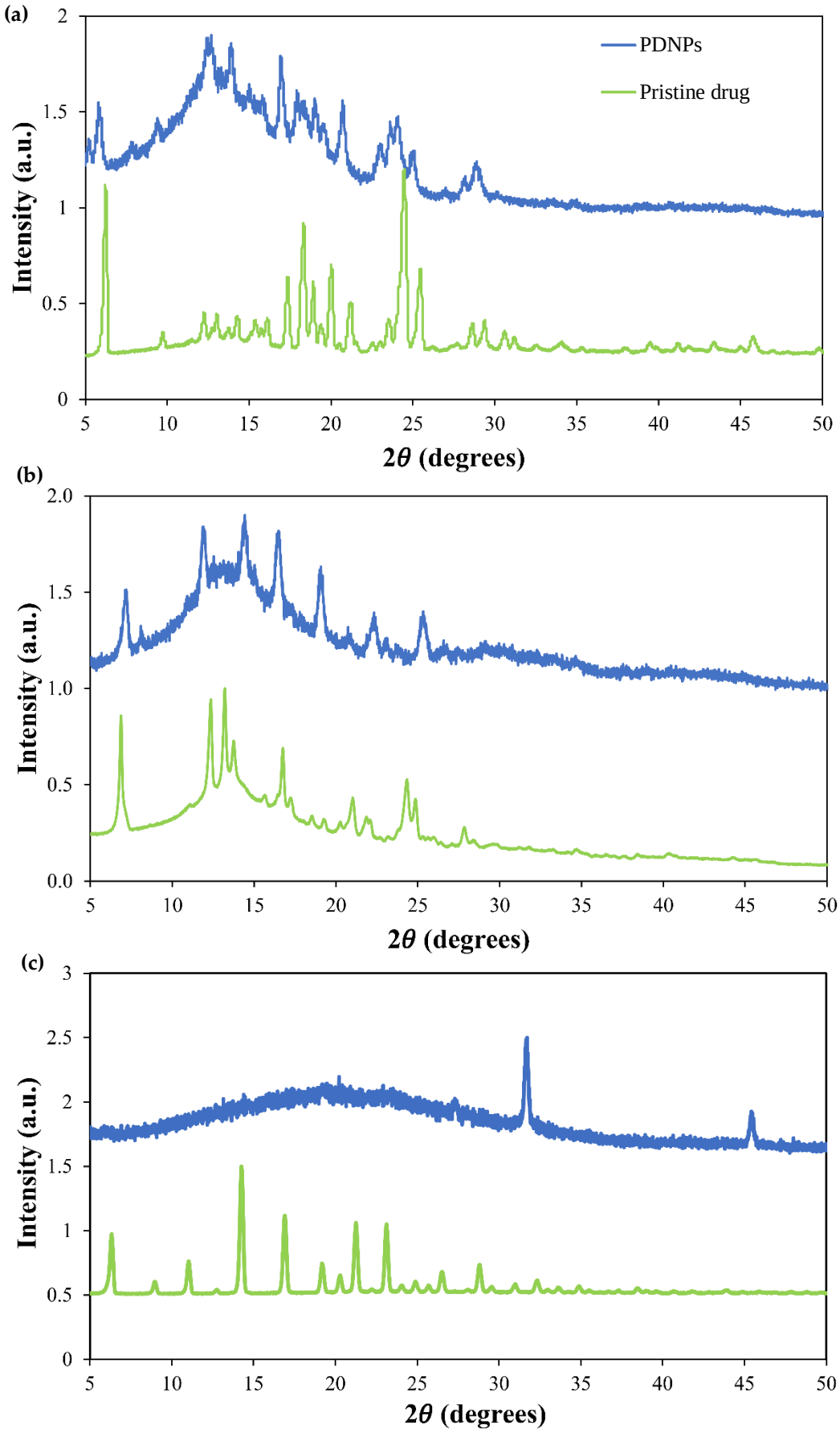

Figure 5. Powder X-ray diffraction patterns of (a) raw and nanonized IMA, (b) raw and nanonized DAS and (c) raw and nanonized TOF.

To support the PXRD results, the thermal behavior of the pristine and nanonized drugs was analyzed by DSC. Pristine IMA showed melting temperature (T_m) at 215 °C (Figure 6). Pristine DAS and TOF showed two melting temperatures at 287 and 318 °C and at 148 and 168 °C, respectively, suggesting the presence of a mixture of different polymorphs [87,88,91]. The transitions in pristine TOF were very weak with very broad peaks (Figure 6). Nanonization led to a decrease of the T_m of IMA to 206°C for IMA and to 280 and 295°C for DAS. In addition, a decrease of the melting enthalpy (Δ_h) of both drugs was observed (Table 3). These results confirm their semi-crystalline nature though with a smaller degree of crystallinity than the pristine counterparts. Pure TOF NPs did not show any thermal transition which confirmed the very low crystallinity of these NPs, in good agreement with PXRD data. The fact that NPs of IMA and DAS resulted in smaller amorphization extent compared with TOF NPs could be attributed to the lower LogP value of TOF. Zhu demonstrated that there is a good correlation between the drug logP value and the particle stability during nanoprecipitation, reporting that drugs characterized by lower logP values (<2) tend to have a more metastable nature in their nanonized form [84]. However, the exact mechanism responsible for the amorphization of crystalline/semi-crystalline drugs upon nanoprecipition remains controversial [92].

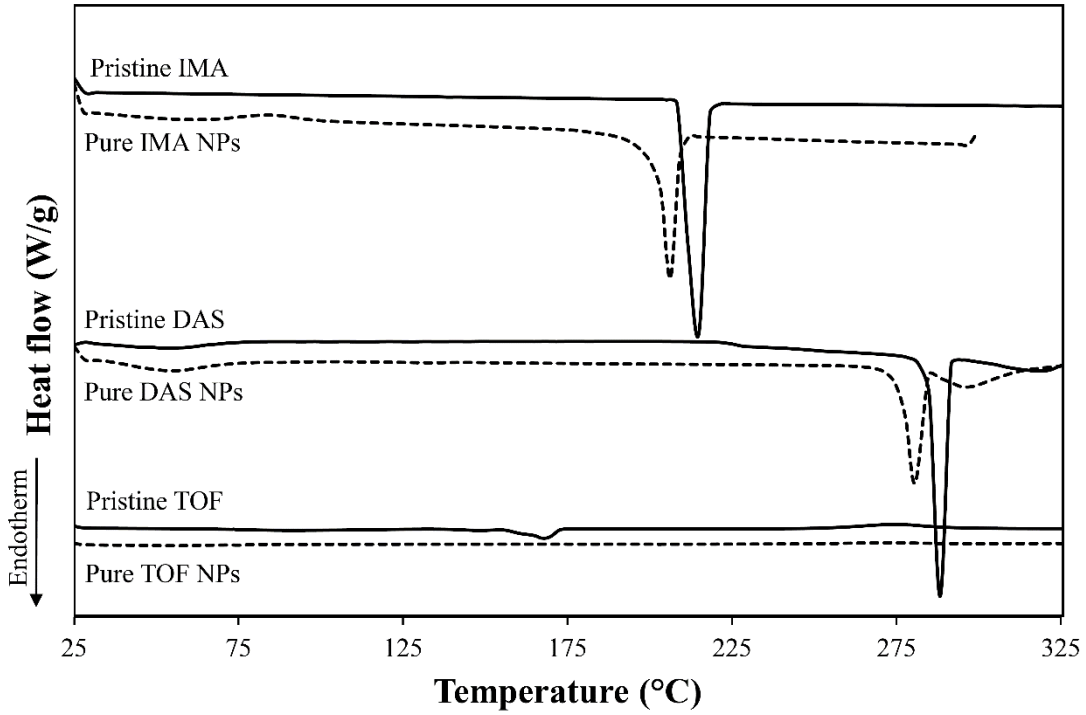

Figure 16. DSC thermograms of pristine and nanonized kinae inhibitors.

Table 3. DSC data of pristine and nanonized IMA, DAS and TOF.

Drug	Form	T_m (°C) [1]	ΔH_m (J/g) [1]
IMA	Raw	215	124
	Nanonized	206	106
DAS	Raw	287/318	89/41
	Nanonized	280/295	53/20
TOF	Raw	148/168	3/52
	Nanonized	N.D.	-

[1] Determined in the heating ramp.
N.D.: Not detected

Then, the morphology of the NPs was visualized by HR-SEM and compared to the unprocessed counterparts. Raw IMA (Figure 7a) and DAS (Figure 7c) showed irregular microparticles within a broad size range, suggesting some amorphousness. Raw TOF showed a more elongated morphology (Figure 7e). All the PDNPs showed smooth, rounded morphology, consistent with their almost intermediate to high amorphous structure [93,94] (Figure 7b,d,f). The size of the NPs was significantly smaller and more uniform than that of the respective raw counterparts. The morphology of the particles suggests that the precipitation process inside the system was fast, allowing the effective trapping of the drug nanoparticles in a less stable amorphous state [9,89,92,95]. These results further emphasize the advantage of the use of flow focusing techniques for the synthesis of additive-free nanodrugs of uniform size with enhanced saturation solubility and dissolution rates.

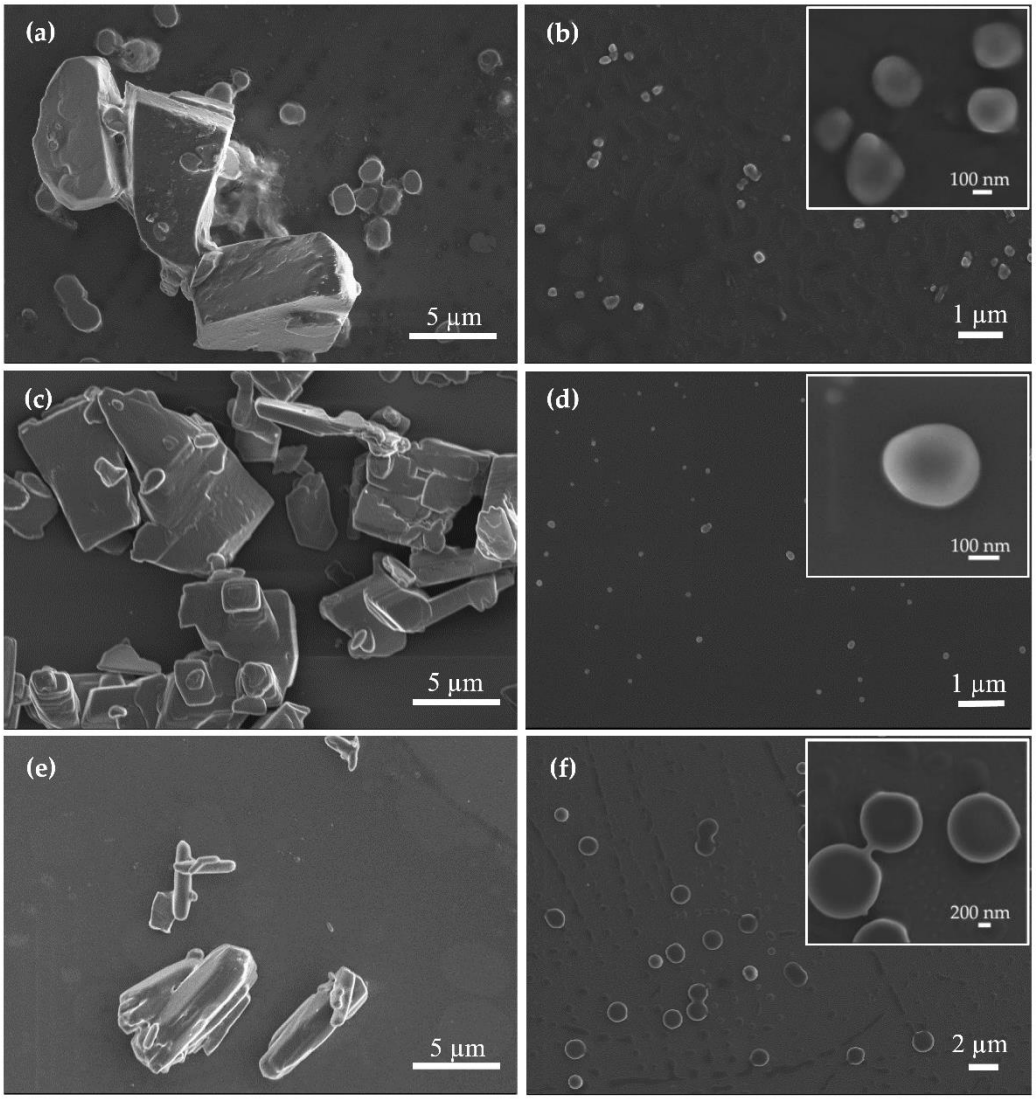

Figure 7. HR-SEM micrographs of (a) raw imatinib versus (a1, a2) imatinib PDNPs, (b) raw dasatinib versus (b1, b2) dasatinib PDNPs and (c) raw tofacitinib versus (c1, c2) tofacitinib PDNPs.

5. Conclusions

In this work, we produced surfactant-free PDNPs of three kinase inhibitors using a simple Si-based microfluidic device was investigated. For this, NPs of three drug candidates, namely IMA, DAS and TOF, were successfully produced and characterized by DLS, DSC, PXRD and HR-SEM.

The first part of this work involved the study of the effect of the variation of different parameters in the microfluidic precipitation process on the size of the synthesized nanoparticles. These parameters included the change in the geometry of the channels, the overall S/AS flow rate, and the ratio between S/AS flow rate with increasing AS flow rate. Results demonstrate that the NP size was controlled and in the nanometric range with monomodal size distribution. In addition, changes in the S/AS flow rate have a strong influence on the size and size distribution of the produced particles. Also, differences in particle size as a function of channel geometry are observed upon the synthesis of IMA and TOF NPs at flow rates at which complete mixing between S and AS is not reached, which leads to the formation of particles with larger size in the T-shaped device.

Following the optimization of the precipitation process, a comparative analysis of the results for each nano-drug and its pristine counterpart was performed. DSC and PXRD analysis revealed that drug nanonization has led to a dramatic decrease in the crystallinity of the raw drug form in good agreement with previous works involving flow focusing techniques for the synthesis of additive-free nanodrug formulations. HR-SEM confirmed that the particles were amorphous in nature as demonstrated by their smooth and spherical shape. Overall, our results show the promise of this device setup to produce PDNPs of poorly water-soluble drugs. Ongoing research investigates the extension of this platform to the synthesis of different types of drug-loaded polymeric NPs and hybrid ceramic/polymer nanomaterials.

Author Contributions: Conceptualization, R.S.A, A.K. and A.S.; experimental work, R.S.A. and Y.R.; data analysis, R.S.A., Y.R. and A.S.; writing—original draft preparation, R.S.A and A.S.; writing—review and editing, R.S.A. and A.S.; All authors have read and agreed to the published version of the manuscript.

Funding: This research was supported by the Ministry of Science and Technology of Israel (grant #3-17339). The authors thank the partial financial support of the Russell Berrie Nanotechnology Center (Technion-Israel Institute of Technology).

Institutional Review Board Statement: Not applicable.

Informed Consent Statement: Not applicable.

Conflicts of Interest: The authors declare no conflicts of interest.

References

1. Müller, R.; Junghanns Nanocrystal technology, drug delivery and clinical applications. *Int. J. Nanomedicine* **2008**, *3*, 295, doi:10.2147/ijn.s595.
2. Calderón, M.; Sosnik, A. *Biotechnology Advances*. 2015, pp. 1277–1278.
3. Alvarez-Lorenzo, C.; Concheiro, A. Smart drug delivery systems: from fundamentals to the clinic. *Chem. Commun.* **2014**, *50*, 7743–7765, doi:10.1039/C4CC01429D.
4. Gao, L.; Zhang, D.; Chen, M. Drug nanocrystals for the formulation of poorly soluble drugs and its application as a potential drug delivery system. *J. Nanoparticle Res.* 2008, *10*, 845–862.
5. Gigliobianco, M.R.; Casadidio, C.; Censi, R.; Di Martino, P. Nanocrystals of poorly soluble drugs: Drug bioavailability and physicochemical stability. *Pharmaceutics* **2018**, *10*, 1–29, doi:10.3390/pharmaceutics10030134.
6. Benet, L.Z. The role of BCS (biopharmaceutics classification system) and BDDCS (biopharmaceutics drug disposition classification system) in drug development. *J. Pharm. Sci.* **2013**, *102*, 34–42, doi:10.1002/jps.23359.
7. Mehta, M.U.; Uppoor, R.S.; Conner, D.P.; Seo, P.; Vaidyanathan, J.; Volpe, D.A.; Stier, E.; Chilukuri, D.; Dorantes, A.; Ghosh, T.; et al. Impact of the US FDA "biopharmaceutics Classification System" (BCS) Guidance on Global Drug Development. *Mol. Pharm.* 2017, *14*, 4334–4338.
8. Müller, R.H.; Keck, C.M. Twenty years of drug nanocrystals: Where are we, and where do we go? *Eur. J. Pharm. Biopharm.* 2012, *80*, 1–3.

9. D'Addio, S.M.; Prud'homme, R.K. Controlling drug nanoparticle formation by rapid precipitation. *Adv. Drug Deliv. Rev.* 2011, *63*, 417–426.
10. Sinha, B.; Müller, R.H.; Möschwitzer, J.P. Bottom-up approaches for preparing drug nanocrystals: Formulations and factors affecting particle size. *Int. J. Pharm.* **2013**, *453*, 126–141, doi:10.1016/j.ijpharm.2013.01.019.
11. Paul, S.M.; Mytelka, D.S.; Dunwiddie, C.T.; Persinger, C.C.; Munos, B.H.; Lindborg, S.R.; Schacht, A.L. How to improve RD productivity: The pharmaceutical industry's grand challenge. *Nat. Rev. Drug Discov.* 2010, *9*, 203–214.
12. Scannell, J.W.; Blanckley, A.; Boldon, H.; Warrington, B. Diagnosing the decline in pharmaceutical R&D efficiency. *Nat. Rev. Drug Discov.* 2012, *11*, 191–200.
13. Sosnik, A.; Augustine, R. Challenges in oral drug delivery of antiretrovirals and the innovative strategies to overcome them. *Adv. Drug Deliv. Rev.* **2016**, *103*, 105–120, doi:10.1016/j.addr.2015.12.022.
14. Rabinow, B.E. Nanosuspensions in drug delivery. *Nat. Rev. Drug Discov.* 2004, *3*, 785–796.
15. Sverdlov Arzi, R.; Sosnik, A. Electrohydrodynamic atomization and spray-drying for the production of pure drug nanocrystals and co-crystals. *Adv. Drug Deliv. Rev.* **2018**, *131*, 79–100, doi:10.1016/j.addr.2018.07.012.
16. Müller, R.H.; Gohla, S.; Keck, C.M. State of the art of nanocrystals - Special features, production, nanotoxicology aspects and intracellular delivery. *Eur. J. Pharm. Biopharm.* 2011, *78*, 1–9.
17. Baba, K.; Nishida, K. Steroid nanocrystals prepared using the nano spray dryer B-90. *Pharmaceutics* **2013**, *5*, 107–114, doi:10.3390/pharmaceutics5010107.
18. Jinno, J.I.; Kamada, N.; Miyake, M.; Yamada, K.; Mukai, T.; Odomi, M.; Toguchi, H.; Liversidge, G.G.; Higaki, K.; Kimura, T. Effect of particle size reduction on dissolution and oral absorption of a poorly water-soluble drug, cilostazol, in beagle dogs. *J. Control. Release* **2006**, *111*, 56–64, doi:10.1016/j.jconrel.2005.11.013.
19. Merisko-Liversidge, E.; Liversidge, G.G.; Cooper, E.R. Nanosizing: A formulation approach for poorly-water-soluble compounds. *Eur. J. Pharm. Sci.* 2003, *18*, 113–120.
20. Keck, C.M.; Müller, R.H. Drug nanocrystals of poorly soluble drugs produced by high pressure homogenisation. *Eur. J. Pharm. Biopharm.* 2006, *62*, 3–16.
21. Kesisoglou, F.; Panmai, S.; Wu, Y. Nanosizing - Oral formulation development and biopharmaceutical evaluation. *Adv. Drug Deliv. Rev.* 2007, *59*, 631–644.
22. Zhang, H.X.; Wang, J.X.; Shao, L.; Chen, J.F. Microfluidic fabrication of monodispersed pharmaceutical colloidal spheres of atorvastatin calcium with tunable sizes. *Ind. Eng. Chem. Res.* **2010**, *49*, 4156–4161, doi:10.1021/ie901365w.
23. El-Say, K.M.; El-Sawy, H.S. Polymeric nanoparticles: Promising platform for drug delivery. *Int. J. Pharm.* 2017, *528*, 675–691.
24. Müller, R.H.; Gohla, S.; Keck, C.M. State of the art of nanocrystals - Special features, production, nanotoxicology aspects and intracellular delivery. *Eur. J. Pharm. Biopharm.* 2011, *78*, 1–9.
25. De Waard, H.; Frijlink, H.W.; Hinrichs, W.L.J. Bottom-up preparation techniques for nanocrystals of lipophilic drugs. *Pharm. Res.* **2011**, *28*, 1220–1223, doi:10.1007/s11095-010-0323-3.
26. Shan, N.; Zaworotko, M.J. The_role_of_cocrystals_in_pharma. *Drug Discov. Today* **2008**, *13*, 440–446, doi:10.1016/J.DRUDIS.2008.03.004.
27. Liu, D.; Zhang, H.; Fontana, F.; Hirvonen, J.T.; Santos, H.A. Current developments and applications of microfluidic technology toward clinical translation of nanomedicines. *Adv. Drug Deliv. Rev.* **2018**, *128*, 54–83, doi:10.1016/j.addr.2017.08.003.
28. Imperiale, J.C.; Bevilacqua, G.; De Rosa, P.T.V.; Sosnik, A. Production of pure indinavir free base nanoparticles by a supercritical anti-solvent (SAS) method. *Drug Dev. Ind. Pharm.* **2014**, *40*, 1607–1615, doi:10.3109/03639045.2013.838581.
29. Imperiale, J.C.; Nejamkin, P.; del Sole, M.J.; Lanusse, C.E.; Sosnik, A. Novel protease inhibitor-loaded Nanoparticle-in-Microparticle Delivery System leads to a dramatic improvement of the oral pharmacokinetics in dogs. *Biomaterials* **2015**, *37*,

383–394, doi:10.1016/j.biomaterials.2014.10.026.

30. Augustine, R.; Ashkenazi, D.L.; Arzi, R.S.; Zlobin, V.; Shofti, R.; Sosnik, A. Nanoparticle-in-microparticle oral drug delivery system of a clinically relevant darunavir/ritonavir antiretroviral combination. *Acta Biomater.* **2018**, *74*, 344–359, doi:10.1016/j.actbio.2018.04.045.
31. Sosnik, A.; Mühlebach, S. Editorial: Drug Nanoparticles and Nano-Cocrystals: From Production and Characterization to Clinical Translation. *Adv. Drug Deliv. Rev.* 2018, *131*, 1–2.
32. Peltonen, L. Practical guidelines for the characterization and quality control of pure drug nanoparticles and nano-cocrystals in the pharmaceutical industry. *Adv. Drug Deliv. Rev.* 2018, *131*, 101–115.
33. Surve, D.H.; Jindal, A.B. Recent advances in long-acting nanoformulations for delivery of antiretroviral drugs. *J. Control. Release* 2020, *324*, 379–404.
34. Lu, Y.; Li, Y.; Wu, W. Injected nanocrystals for targeted drug delivery. *Acta Pharm. Sin. B* 2016, *6*, 106–113.
35. Fessi, H.; Puisieux, F.; Devissaguet, J.P.; Ammoury, N.; Benita, S. Nanocapsule formation by interfacial polymer deposition following solvent displacement. *Int. J. Pharm.* **1989**, doi:10.1016/0378-5173(89)90281-0.
36. Beck-Broichsitter, M.; Rytting, E.; Lebhardt, T.; Wang, X.; Kissel, T. Preparation of nanoparticles by solvent displacement for drug delivery: A shift in the " ouzo region" upon drug loading. *Eur. J. Pharm. Sci.* **2010**, *41*, 244–253, doi:10.1016/j.ejps.2010.06.007.
37. Ding, S.; Anton, N.; Vandamme, T.F.; Serra, C.A. Microfluidic nanoprecipitation systems for preparing pure drug or polymeric drug loaded nanoparticles: an overview. *Expert Opin. Drug Deliv.* 2016, *13*, 1447–1460.
38. Thorat, A.A.; Dalvi, S. V. Liquid antisolvent precipitation and stabilization of nanoparticles of poorly water soluble drugs in aqueous suspensions: Recent developments and future perspective. *Chem. Eng. J.* 2012, *181–182*, 1–34.
39. Dashtimoghadam, E.; Mirzadeh, H.; Taromi, F.A.; Nyström, B. Microfluidic self-assembly of polymeric nanoparticles with tunable compactness for controlled drug delivery. *Polymer (Guildf).* **2013**, *54*, 4972–4979, doi:10.1016/j.polymer.2013.07.022.
40. Martins, J.P.; Torrieri, G.; Santos, H.A. The importance of microfluidics for the preparation of nanoparticles as advanced drug delivery systems. *Expert Opin. Drug Deliv.* 2018, *15*, 469–479.
41. Junghanns, J.U.A.H.; Müller, R.H.; Junghanns, J.U.A.H. Nanocrystal technology, drug delivery and clinical applications. *Int. J. Nanomedicine* **2008**, *3*, 295–309, doi:10.2147/IJN.S595.
42. Abdelwahed, W.; Degobert, G.; Stainmesse, S.; Fessi, H. Freeze-drying of nanoparticles: Formulation, process and storage considerations. *Adv. Drug Deliv. Rev.* **2006**, *58*, 1688–1713, doi:10.1016/j.addr.2006.09.017.
43. Fuhrmann, K.; Połomska, A.; Aeberli, C.; Castagner, B.; Gauthier, M.A.; Leroux, J.C. Modular design of redox-responsive stabilizers for nanocrystals. *ACS Nano* **2013**, *7*, 8243–8250, doi:10.1021/nn4037317.
44. Kipp, J.E. The role of solid nanoparticle technology in the parenteral delivery of poorly water-soluble drugs. *Int. J. Pharm.* 2004, *284*, 109–122.
45. Karnik, R.; Gu, F.; Basto, P.; Cannizzaro, C.; Dean, L.; Kyei-Manu, W.; Langer, R.; Farokhzad, O.C. Microfluidic platform for controlled synthesis of polymeric nanoparticles. *Nano Lett.* **2008**, *8*, 2906–2912, doi:10.1021/nl801736q.
46. Whitesides, G.M. The origins and the future of microfluidics. *Nature* 2006, *442*, 368–373.
47. Yi, C.; Li, C.W.; Ji, S.; Yang, M. Microfluidics technology for manipulation and analysis of biological cells. *Anal. Chim. Acta* 2006, *560*, 1–23.
48. Choi, N.W.; Cabodi, M.; Held, B.; Gleghorn, J.P.; Bonassar, L.J.; Stroock, A.D. Microfluidic scaffolds for tissue engineering. *Nat. Mater.* **2007**, *6*, 908–915, doi:10.1038/nmat2022.
49. Damiati, S.; Kompella, U.B.; Damiati, S.A.; Kodzius, R. Microfluidic devices for drug delivery systems and drug screening. *Genes (Basel).* 2018, *9*.
50. Kleinstreuer, C.; Li, J.; Koo, J. Microfluidics of nano-drug delivery. *Int. J. Heat Mass Transf.* **2008**, *51*, 5590–5597,

doi:10.1016/j.ijheatmasstransfer.2008.04.043.

51. Karnik, R.; Gu, F.; Basto, P.; Cannizzaro, C.; Dean, L.; Kyei-Manu, W.; Langer, R.; Farokhzad, O.C. Microfluidic platform for controlled synthesis of polymeric nanoparticles. *Nano Lett.* **2008**, *8*, 2906–2912, doi:10.1021/nl801736q.
52. Valencia, P.M.; Pridgen, E.M.; Rhee, M.; Langer, R.; Farokhzad, O.C.; Karnik, R. Microfluidic platform for combinatorial synthesis and optimization of targeted nanoparticles for cancer therapy. *ACS Nano* **2013**, *7*, 10671–10680, doi:10.1021/nn403370e.
53. Rahimi, M.; Valeh-e-Sheyda, P.; Rashidi, H. Statistical optimization of curcumin nanosuspension through liquid anti-solvent precipitation (LASP) process in a microfluidic platform: Box-Behnken design approach. *Korean J. Chem. Eng.* **2017**, *34*, 3017–3027, doi:10.1007/s11814-017-0201-3.
54. Ali, H.S.M.; York, P.; Blagden, N. Preparation of hydrocortisone nanosuspension through a bottom-up nanoprecipitation technique using microfluidic reactors. *Int. J. Pharm.* **2009**, *375*, 107–113, doi:10.1016/j.ijpharm.2009.03.029.
55. Fontana, F.; Figueiredo, P.; Zhang, P.; Hirvonen, J.T.; Liu, D.; Santos, H.A. Production of pure drug nanocrystals and nano co-crystals by confinement methods. *Adv. Drug Deliv. Rev.* 2018, *131*, 3–21.
56. Ding, S.; Anton, N.; Vandamme, T.F.; Serra, C.A. Microfluidic nanoprecipitation systems for preparing pure drug or polymeric drug loaded nanoparticles: an overview. *Expert Opin. Drug Deliv.* 2016.
57. Zhang, Q.X.; Xu, L.M.; Zhou, Y.; Wang, J.X.; Chen, J.F. Preparation of drug nanoparticles using a T-junction microchannel system. *Ind. Eng. Chem. Res.* **2011**, *50*, 13805–13812, doi:10.1021/ie201291r.
58. Liu, D.; Zhang, H.; Fontana, F.; Hirvonen, J.T.; Santos, H.A. Microfluidic-assisted fabrication of carriers for controlled drug delivery. *Lab Chip* 2017, *17*, 1856–1883.
59. Duncanson, W.J.; Lin, T.; Abate, A.R.; Seiffert, S.; Shah, R.K.; Weitz, D.A. Microfluidic synthesis of advanced microparticles for encapsulation and controlled release. *Lab Chip* 2012, *12*, 2135–2145.
60. Gross, S.; Rahal, R.; Stransky, N.; Lengauer, C.; Hoeflich, K.P. Targeting cancer with kinase inhibitors. *J. Clin. Invest.* 2015, *125*, 1780–1789.
61. Bhullar, K.S.; Lagarón, N.O.; McGowan, E.M.; Parmar, I.; Jha, A.; Hubbard, B.P.; Rupasinghe, H.P.V. Kinase-targeted cancer therapies: Progress, challenges and future directions. *Mol. Cancer* 2018, *17*.
62. Wu, P.; Nielsen, T.E.; Clausen, M.H. FDA-approved small-molecule kinase inhibitors. *Trends Pharmacol. Sci.* 2015, *36*, 422–439.
63. Pottier, C.; Fresnais, M.; Gilon, M.; Jérusalem, G.; Longuespée, R.; Sounni, N.E. Tyrosine kinase inhibitors in cancer: Breakthrough and challenges of targeted therapy. *Cancers (Basel).* 2020, *12*.
64. Herbrink, M.; Nuijen, B.; Schellens, J.H.M.; Beijnen, J.H. Variability in bioavailability of small molecular tyrosine kinase inhibitors. *Cancer Treat. Rev.* 2015, *41*, 412–422.
65. Umazume, K.; Liu, L.H.; Scott, P.A.; Fernandez de Castro, J.P.; McDonald, K.; Kaplan, H.J.; Tamiya, S. Inhibition of PVR with a tyrosine kinase inhibitor, dasatinib, in the swine. *Investig. Ophthalmol. Vis. Sci.* **2013**, *54*, 1150–1159, doi:10.1167/iovs.12-10418.
66. Chen, S.Y.; Shiau, A.L.; Wu, C.L.; Wang, C.R. Amelioration of experimental arthritis by the intra-articular injection of an epidermal growth factor receptor tyrosine kinase inhibitor. *Clin. Exp. Rheumatol.* **2015**, *33*, 839–843.
67. Smidova, V.; Michalek, P.; Goliasova, Z.; Eckschlager, T.; Hodek, P.; Adam, V.; Heger, Z. Nanomedicine of tyrosine kinase inhibitors. *Theranostics* 2021, *11*, 1546–1567.
68. Roskoski, R. Properties of FDA-approved small molecule protein kinase inhibitors: A 2020 update. *Pharmacol. Res.* 2020, *152*.
69. Committee for Human Medicinal Products ICH guideline Q3C (R5) on impurities: Guideline for Residual Solvents. *Int. Conf. Harmon. Tech. Requir. Regist. Pharm. Hum. Use* **2015**, *44*, 24.
70. Bukchin, A.; Kuplennik, N.; Carcaboso, Á.M.; Sosnik, A. Effect of growing glycosylation extents on the self-assembly and active targeting in vitro of branched poly(ethylene oxide)-poly(propylene oxide) block copolymers. *Appl. Mater. Today* **2018**,

11, 57–69, doi:10.1016/j.apmt.2018.01.003.

71. Nicolaou, K.C.; Vourloumis, D.; Totokotsopoulos, S.; Papakyriakou, A.; Karsunky, H.; Fernando, H.; Gavrilyuk, J.; Webb, D.; Stepan, A.F. Synthesis and Biopharmaceutical Evaluation of Imatinib Analogues Featuring Unusual Structural Motifs. *ChemMedChem* **2016**, *11*, 31–37, doi:10.1002/cmdc.201500510.
72. Bukchin, A.; Pascual-Pasto, G.; Cuadrado-Vilanova, M.; Castillo-Ecija, H.; Monterrubio, C.; Olaciregui, N.G.; Vila-Ubach, M.; Ordeix, L.; Mora, J.; Carcaboso, A.M.; et al. Glucosylated nanomicelles target glucose-avid pediatric patient-derived sarcomas. *J. Control. Release* **2018**, *276*, 59–71, doi:10.1016/j.jconrel.2018.02.034.
73. Kamath, A. V.; Wang, J.; Lee, F.Y.; Marathe, P.H. Preclinical pharmacokinetics and in vitro metabolism of dasatinib (BMS-354825): A potent oral multi-targeted kinase inhibitor against SRC and BCR-ABL. *Cancer Chemother. Pharmacol.* **2008**, *61*, 365–376, doi:10.1007/s00280-007-0478-8.
74. Seo, S.; Suh, W. Antiangiogenic effect of dasatinib in murine models of oxygen-induced retinopathy and laser-induced choroidal neovascularization. *Mol. Vis.* **2017**, *23*, 823–831.
75. Haralampiev, I.; Alonso de Armiño, D.J.; Luck, M.; Fischer, M.; Abel, T.; Huster, D.; Di Lella, S.; Scheidt, H.A.; Müller, P. Interaction of the small-molecule kinase inhibitors tofacitinib and lapatinib with membranes. *Biochim. Biophys. Acta - Biomembr.* **2020**, *1862*, doi:10.1016/j.bbamem.2020.183414.
76. Dhillon, S. Tofacitinib: A Review in Rheumatoid Arthritis. *Drugs* **2017**, *77*, 1987–2001, doi:10.1007/s40265-017-0835-9.
77. Biemans, V.B.C.; Sleutjes, J.A.M.; de Vries, A.C.; Bodelier, A.G.L.; Dijkstra, G.; Oldenburg, B.; Löwenberg, M.; van Bodegraven, A.A.; van der Meulen-de Jong, A.E.; de Boer, N.K.H.; et al. Tofacitinib for ulcerative colitis: results of the prospective Dutch Initiative on Crohn and Colitis (ICC) registry. *Aliment. Pharmacol. Ther.* **2020**, *51*, 880–888, doi:10.1111/apt.15689.
78. Liu, D.; Cito, S.; Zhang, Y.; Wang, C.F.; Sikanen, T.M.; Santos, H.A. A versatile and robust microfluidic platform toward high throughput synthesis of homogeneous nanoparticles with tunable properties. *Adv. Mater.* **2015**, *27*, 2298–2304, doi:10.1002/adma.201405408.
79. Tao, J.; Chow, S.F.; Zheng, Y. Application of flash nanoprecipitation to fabricate poorly water-soluble drug nanoparticles. *Acta Pharm. Sin. B* 2019, *9*, 4–18.
80. Zhao, H.; Wang, J.X.; Wang, Q.A.; Chen, J.F.; Yun, J. Controlled liquid antisolvent precipitation of hydrophobic pharmaceutical nanoparticles in a MicroChannel reactor. *Ind. Eng. Chem. Res.* **2007**, *46*, 8229–8235, doi:10.1021/ie070498e.
81. Zhu, W.Z.; Wang, J.X.; Shao, L.; Zhang, H.X.; Zhang, Q.X.; Chen, J.F. Liquid antisolvent preparation of amorphous cefuroxime axetil nanoparticles in a tube-in-tube microchannel reactor. *Int. J. Pharm.* **2010**, *395*, 260–265, doi:10.1016/j.ijpharm.2010.05.018.
82. Zhang, S. h.; Yun, J.; Shen, S.; Chen, Z.; Yao, K. j.; Chen, J.; Chen, B. Formation of solid lipid nanoparticles in a microchannel system with a cross-shaped junction. *Chem. Eng. Sci.* **2008**, *63*, 5600–5605, doi:10.1016/j.ces.2008.08.005.
83. Wang, J.X.; Zhang, Q.X.; Zhou, Y.; Shao, L.; Chen, J.F. Microfluidic synthesis of amorphous cefuroxime axetil nanoparticles with size-dependent and enhanced dissolution rate. *Chem. Eng. J.* **2010**, *162*, 844–851, doi:10.1016/j.cej.2010.06.022.
84. Zhu, Z. Flash nanoprecipitation: Prediction and enhancement of particle stability via drug structure. *Mol. Pharmaceutics* **2014**, *11*, 776–786, doi:10.1021/mp500025e.
85. Wu, L.; Zhang, J.; Watanabe, W. Physical and chemical stability of drug nanoparticles. *Adv. Drug Deliv. Rev.* 2011, *63*, 456–469.
86. Van Den Mooter, G. The use of amorphous solid dispersions: A formulation strategy to overcome poor solubility and dissolution rate. *Drug Discov. Today Technol.* 2012, *9*.
87. Younis, U.S.; Vallorz, E.; Addison, K.J.; Ledford, J.G.; Myrdal, P.B. Preformulation and Evaluation of Tofacitinib as a Therapeutic Treatment for Asthma. *AAPS PharmSciTech* **2019**, *20*, doi:10.1208/s12249-019-1377-0.

88. Ren, P.; Martin, M.; Worrall, C.P.; del Rio Gancedo, S. Kinase Inhibitor Polymorphs 2015, 1–54.
89. Hancock, B.C.; Parks, M. What is the true solubility advantage for amorphous pharmaceuticals? *Pharm. Res.* **2000**, *17*, 397–404, doi:10.1023/A:1007516718048.
90. Yang, W.; Johnston, K.P.; Williams, R.O. Comparison of bioavailability of amorphous versus crystalline itraconazole nanoparticles via pulmonary administration in rats. *Eur. J. Pharm. Biopharm.* **2010**, *75*, 33–41, doi:10.1016/j.ejpb.2010.01.011.
91. Simo, O.; Filipcik, J.; Martaus, A.; Jegorov, A.; Gavenda, A.; Aronhime, J.; Vraspir, P.; Koltai, T.; Faustmann, J.; Gabriel, R. Polymorphs of dasatinib and process for preparation thereof. *PCT Int. Appl.* 2009.
92. Lepeltier, E.; Bourgaux, C.; Couvreur, P. Nanoprecipitation and the "Ouzo effect": Application to drug delivery devices. *Adv. Drug Deliv. Rev.* 2014, *71*, 86–97.
93. Jog, R.; Burgess, D.J. Pharmaceutical Amorphous Nanoparticles. *J. Pharm. Sci.* 2017, *106*, 39–65.
94. Mehenni, L.; Lahiani-Skiba, M.; Ladam, G.; Hallouard, F.; Skiba, M. Preparation and characterization of spherical amorphous solid dispersion with amphotericin B. *Pharmaceutics* **2018**, *10*, doi:10.3390/pharmaceutics10040235.
95. Schianti, J.N.; Cerize, N.N.P.; de Oliveira, A.M.; Derenzo, S.; Seabra, A.C.; Góngora-Rubio, M.R. Rifampicin nanoprecipitation using flow focusing microfluidic device. *J. Nanomedicine Nanotechnol.* **2013**, *4*, doi:10.4172/2157-7439.1000172.